











## RESEARCH ARTICLE

10.1029/2024GC011816

# Tracing a Mantle Component in Both Paleo and Modern Fluids Along Seismogenic Faults of Southern Italy

Filippo Zummo<sup>1</sup> , Fabrizio Agosta<sup>1</sup> , Antonio M. Álvarez-Valero<sup>2</sup>, Andrea Billi<sup>3</sup> , Dario Buttitta<sup>4</sup> , Antonio Caracausi<sup>2,4</sup> , Gabriele Carnevale<sup>4</sup> , Barbara Marchesini<sup>3,5</sup> , and Michele Paternoster<sup>1,4</sup> 

<sup>1</sup>Dipartimento di Scienze, Università della Basilicata, Potenza, Italy, <sup>2</sup>Departamento de Geología, Universidad de Salamanca, Salamanca, Spain, <sup>3</sup>Cnr-Istituto di Geologia Ambientale e Geoingegneria, Rome, Italy, <sup>4</sup>Istituto Nazionale di Geofisica e Vulcanologia, Palermo, Italy, <sup>5</sup>Dipartimento di Scienze della terra, Sapienza Università di Roma, Roma, Italy

### Key Points:

- Paleofluids in the studied seismogenic fault derive from the mixing between crustal and mantle (~20%) derived fluids
- The variability of the He isotopic signature registered in fluid inclusions results from either early trapping processes (due to past possible earthquakes events) or post trapping processes by addition of radiogenic <sup>4</sup>He produced within fractured calcite veins over time (vein aging)
- The pristine mantle source has been active in the Irpinia area (southern Italy) for at least 1 Ma based on the post trapping process

### Supporting Information:

Supporting Information may be found in the online version of this article.

### Correspondence to:

F. Zummo,  
filippo.zummo@unibas.it

### Citation:

Zummo, F., Agosta, F., Álvarez-Valero, A. M., Billi, A., Buttitta, D., Caracausi, A., et al. (2024). Tracing a mantle component in both paleo and modern fluids along seismogenic faults of southern Italy. *Geochemistry, Geophysics, Geosystems*, 25, e2024GC011816. <https://doi.org/10.1029/2024GC011816>

Received 13 AUG 2024

Accepted 26 OCT 2024

### Author Contributions:

**Conceptualization:** Filippo Zummo, Fabrizio Agosta, Antonio M. Álvarez-Valero, Andrea Billi, Dario Buttitta, Antonio Caracausi, Gabriele Carnevale, Barbara Marchesini, Michele Paternoster  
**Data curation:** Filippo Zummo, Fabrizio Agosta, Antonio M. Álvarez-Valero, Andrea Billi, Antonio Caracausi, Michele Paternoster

© 2024 The Author(s). *Geochemistry, Geophysics, Geosystems* published by Wiley Periodicals LLC on behalf of American Geophysical Union. This is an open access article under the terms of the [Creative Commons Attribution License](https://creativecommons.org/licenses/by/4.0/), which permits use, distribution and reproduction in any medium, provided the original work is properly cited.

**Abstract** Aiming at understanding the source of the fluids that mineralizing within seismically active fault zones, we investigate the noble gas isotopes (i.e., helium (He), neon (Ne), and argon (Ar)) in the fluid inclusions (FIs) trapped in the calcite veins sampled along high-angle fault zones of the Contursi hydrothermal basin, southern Italy. The latter basin lies in close vicinity of the  $M_W = 6.9$ , 1980 Irpinia earthquake and exposes numerous fault scarps dissecting Mesozoic shallow-water carbonates. The analyses of noble gases (He, Ne, Ar) are conducted to identify the origin of the volatiles circulating along the faults at the time of calcite precipitation. Then, outcomes of these discussions are compared with currently outgassing of deep-sourced CO<sub>2</sub> coupled to mantle-derived He in that area, whose output is larger than those from some volcanic areas worldwide. The results indicate that He in FIs is dominated by a crustal radiogenic component (<sup>4</sup>He), and by an up to 20% of a mantle-derived component (<sup>3</sup>He), with a highest isotopic signature of 1.38 Ra. This value is consistent with the highest percentage of mantle-derived He associated to high-flux CO<sub>2</sub> gas emission in the investigated area (1.41 Ra). We propose that the variability of the He isotopic signature measured in primary FIs can result from early trapping of fluid inclusions or post trapping processes and seismic activity that modify the pristine He isotopic signature (i.e., derived from the crust and/or mantle) in groundwater along the faults during periods of background seismicity. Such investigations are fundamental to understand fluid migration in fault systems and the role of fluids in processes of earthquake nucleation.

## 1. Introduction

Worldwide, regions characterized by high magnitudes earthquakes such as California, USA, SW Japan, the Anatolian Plateau, Turkey, eastern Tibetan Plateau and both Belice and Irpinia in Italy, exhibit a crustal <sup>4</sup>He released from the seismogenic faults diluted with a mantle-derived He component (Boles et al., 2015; Caracausi et al., 2005; Dogan et al., 2009; Italiano et al., 2000; Kulongoski et al., 2013; Liu et al., 2023; Sano et al., 2016; Zhang et al., 2021). Recently, it has been shown that this dilution varies spatially in accordance with the distribution of seismicity (Caracausi et al., 2022). Moreover, such a dilution might also vary over time as observed during the Kumamoto 2016 earthquake (Japan, Mw = 7.3), reflecting the earthquake magnitude, the host rock lithology, and the seismic cycle (Sano et al., 2016). In the study area (Irpinia, southern Italy), the active faults form pathways that efficiently transfer deep-seated fluids at shallow crustal levels (Buttitta et al., 2023; Caracausi & Paternoster, 2015). Such a transfer is likely due to the volumes of fault-related fractures encompassing the cataclastic fault rocks and major slip surfaces, which act as efficient fluid conduit for fault-parallel flow (Faulkner & Armitage, 2013). In carbonates, within host rocks similar to those exposed in the Irpinia area, the high-angle extensional faults often exhibit high values of secondary porosity and permeability (Agosta et al., 2009; Giuffrida et al., 2020; Smeraglia et al., 2022), and fault rocks with lower values of both porosity and permeability (Ferraro et al., 2020). As such, the fractured fault-related volumes might form volumetrically thick hydraulic conduits allowing fluids to ascend from the Earth's interior toward the atmosphere as documented by integrated geological and geochemical analyses (Caracausi et al., 2022; Curzi et al., 2022). The fault-related fluid circulation in the upper crust can be governed by the spatio-temporal evolution of deformation and associated structural diagenesis of the fault rocks and associated fault-related fractured rock volumes (Balsamo et al., 2016; Ferraro et al., 2020; Sibson, 2000). Such an evolution is forming an even more puzzling problem if associated with the seismic cycles characterizing active faults. This makes challenging to interpret the episodes of fluid ascendance from depth along seismically active fault zones. For this reason, the analysis of fault-related

**Formal analysis:** Filippo Zummo, Fabrizio Agosta, Antonio Caracausi, Gabriele Carnevale, Barbara Marchesini  
**Funding acquisition:** Antonio Caracausi, Michele Paternoster  
**Investigation:** Filippo Zummo, Fabrizio Agosta, Antonio M. Álvarez-Valero, Antonio Caracausi, Michele Paternoster  
**Methodology:** Filippo Zummo, Fabrizio Agosta, Antonio M. Álvarez-Valero, Andrea Billi, Dario Buttitta, Antonio Caracausi, Michele Paternoster  
**Project administration:** Michele Paternoster  
**Resources:** Antonio M. Álvarez-Valero, Antonio Caracausi, Michele Paternoster  
**Software:** Filippo Zummo, Dario Buttitta, Gabriele Carnevale, Barbara Marchesini  
**Supervision:** Antonio Caracausi, Michele Paternoster  
**Validation:** Filippo Zummo, Fabrizio Agosta, Antonio M. Álvarez-Valero, Andrea Billi, Barbara Marchesini, Michele Paternoster  
**Visualization:** Filippo Zummo, Fabrizio Agosta, Antonio M. Álvarez-Valero, Andrea Billi, Dario Buttitta, Gabriele Carnevale, Barbara Marchesini, Michele Paternoster  
**Writing – original draft:** Filippo Zummo, Antonio Caracausi  
**Writing – review & editing:** Filippo Zummo, Fabrizio Agosta, Antonio M. Álvarez-Valero, Antonio Caracausi, Michele Paternoster

mineralization is key to assess the fluid origin, the modalities of fluid circulation through the fault zones, and the extent of fluid-rock interactions (Agosta & Kirschner, 2003; Buttitta et al., 2023; Marchesini et al., 2022; Randazzo et al., 2021; Smeraglia et al., 2016, 2018).

In the analysis of the fault rocks and fault-related fractures exhumed from greater depths form shallow crustal levels, the dilution of deep-seated fluids with the local groundwater might mask the original isotopic signature of the former fluids. In fact, the reactive volatiles (e.g., CO<sub>2</sub>) dissolved in water are speciated (e.g., carbonate equilibrium), and their concentration and isotopic composition are modified by water-gas-rock interaction processes and solute precipitation (Gilfillan et al., 2009). In this regard, noble gases, chemically inert elements, are excellent tracers of both fluid sources and physical processes within the crust (Caracausi & Paternoster, 2015; Curzi et al., 2022; Kendrick & Burnard, 2013; Pik & Marty, 2009). He is the lightest noble gas (Ozima & Podosek, 2002 and reference therein) and in natural fluids, it is present as <sup>3</sup>He and <sup>4</sup>He isotopes, with the former being mainly primordial and stored in the mantle, and the latter being continuously produced by the decay of U and Th (Ozima & Podosek, 2002). In stable continental regions, the He flux is dominated by the radiogenic <sup>4</sup>He produced in the crust (O’Nions & Oxburgh, 1988). In contrast, the primordial <sup>3</sup>He escapes into the atmosphere in tectonically active regions and/or in areas characterized by volcanic activity (Boles et al., 2015; Caracausi & Sulli, 2019; O’Nions & Oxburgh, 1983). As such, the <sup>3</sup>He/<sup>4</sup>He isotope ratio is a powerful tool for recognizing mantle and crust components in the absence of other geological and geochemical evidence (Caracausi & Sulli, 2019; O’Nions & Oxburgh, 1988).

In this work, we investigate the mineralization present within seismically active fault zones. After field and microstructural investigation, we focus on the fluid inclusions (FIs) trapped within calcite veins sampled along high-angle faults exposed in the Contursi hydrothermal basin and surrounding outcrops of the Irpinia region, southern Italy (Figures 1 and 2). The Contursi basin is characterized by a high seismogenic potential (Slejko et al., 1998), and currently background seismicity (Mw < 4 <http://isnet-bulletin.fisica.unina.it/cgi-bin/isnet-events/isnet.cgi>). This basin is very close to the epicentral area of the Mw 6.9 Irpinia earthquake (November 1980, Bernard & Zollo, 1989), which is between 1 and 5 km away from the Contursi town. The seismic volume responsible of the 1980 earthquake is characterized by high values of fracture porosity, and by saturated fractures (Amoroso et al., 2014, 2017). At Contursi, the low-enthalpy hydrothermal system characterized by a water temperature in between 26 and 47°C (Gori et al., 2023) allows the current mantle-derived He outgassing (Buttitta et al., 2023; Italiano et al., 2000). Furthermore, the nearby Mefite D’Ansanto gas emission site, about 30 km away from Contursi, shows a high heat flow with values up to ca. 215 mW/m<sup>2</sup> (Doglioni et al., 1996) and <sup>3</sup>He/<sup>4</sup>He ratios up to 2.84 Ra, which is like those characterizing the active volcanoes in the Campania region of Italy (Vesuvio and Campi Flegrei), about 80 km away.

This study first focuses on the composition, origin, and circulation paths of the mineralizing paleofluids. The results are compared with information derived from the present-day outgassing of the Irpinia area to assess the origin of the mineralizing fluids. In particular, by focusing on He, Ne, Ar isotopes and their isotopes ratios, the possible role exerted by high-angle faults on the ascendance of deep-seated fluids and their possible mixing with meteoric-derived fluids is discussed in light of the available bibliography. We believe that the original results of this study provide new insights into the processes regulating paleo and modern fluid degassing and relationships with the seismicity and crustal deformation in tectonically active continental regions. Understanding these relationships is a crucial factor for unveiling the circulation and upwelling modes of the fluids in the crust over time and the propagation of seismogenic faults and their modes and timing of activation. Consequently, the study of paleofluids and current outgassing fluids associated with a seismic fault helps us to better understand the mechanisms of fluid circulation during the phases of fault activity, but also to understand how geochemical data may have changed due to modifications and post-trapping and/or mixing processes. For sure, multidisciplinary studies can furnish an answer upon long time monitoring. In this region, the IRPINIA Near Fault Observatory, was established, so for sure it is an ideal area to get answers about the relationships between crustal deformations, earthquakes and fluids.

## 2. Geological Setting

The study area is located in the western portion of the southern Apennines fold-and-thrust belt (Figure 1a). This belt developed since Oligo-Miocene times due to the progressive collision between the African and European plates, and interactions with the intervening Adria-Apulia plate (Patacca et al., 1990). Regional-scale thrusting



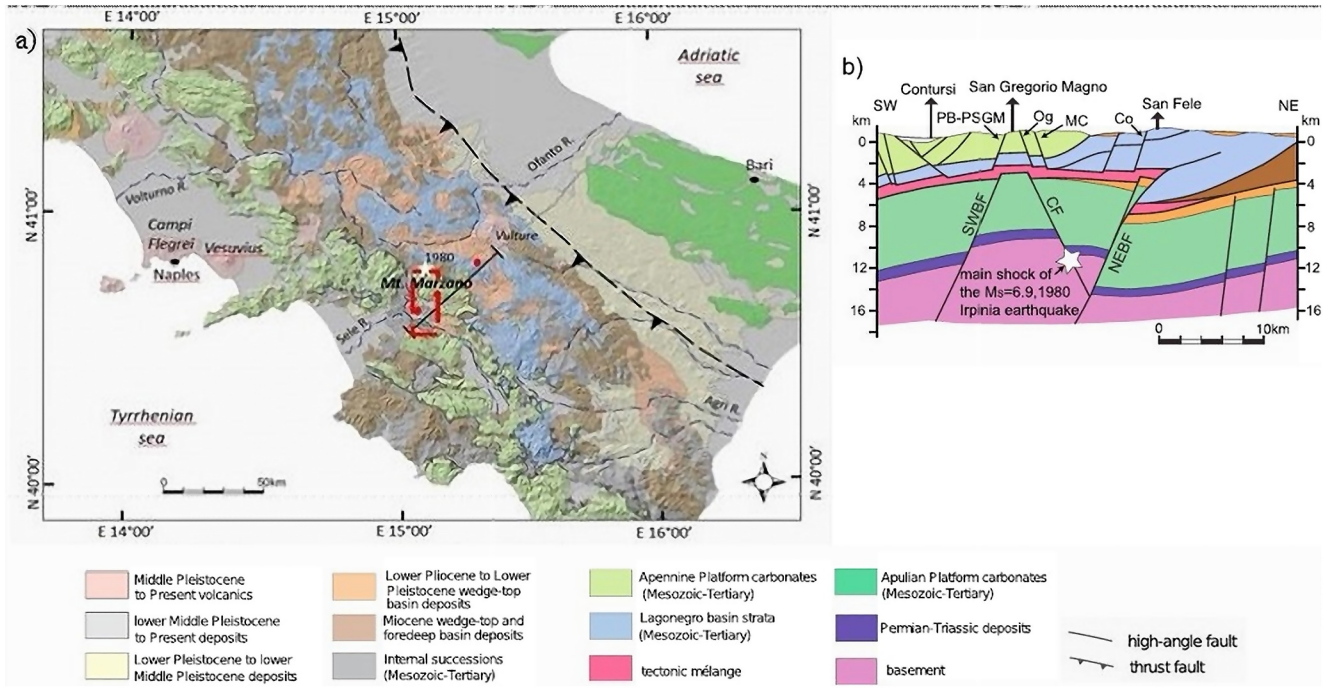


**Figure 1.** Tectonic setting of the 1980 Irpinia earthquake. (a) Geological map of the southern Apennines. The dashed red rectangle indicates the area of interest in this study (modified from Ascione et al., 2013). (b) Cross-section of the study area (after Ascione et al., 2013). The star indicates the hypocenter of the 1980 Irpinia earthquake ( $M_w = 6.9$ ). SWBF, SW Boundary Fault; CF, Central Fault; NEBF, NE Boundary Fault.

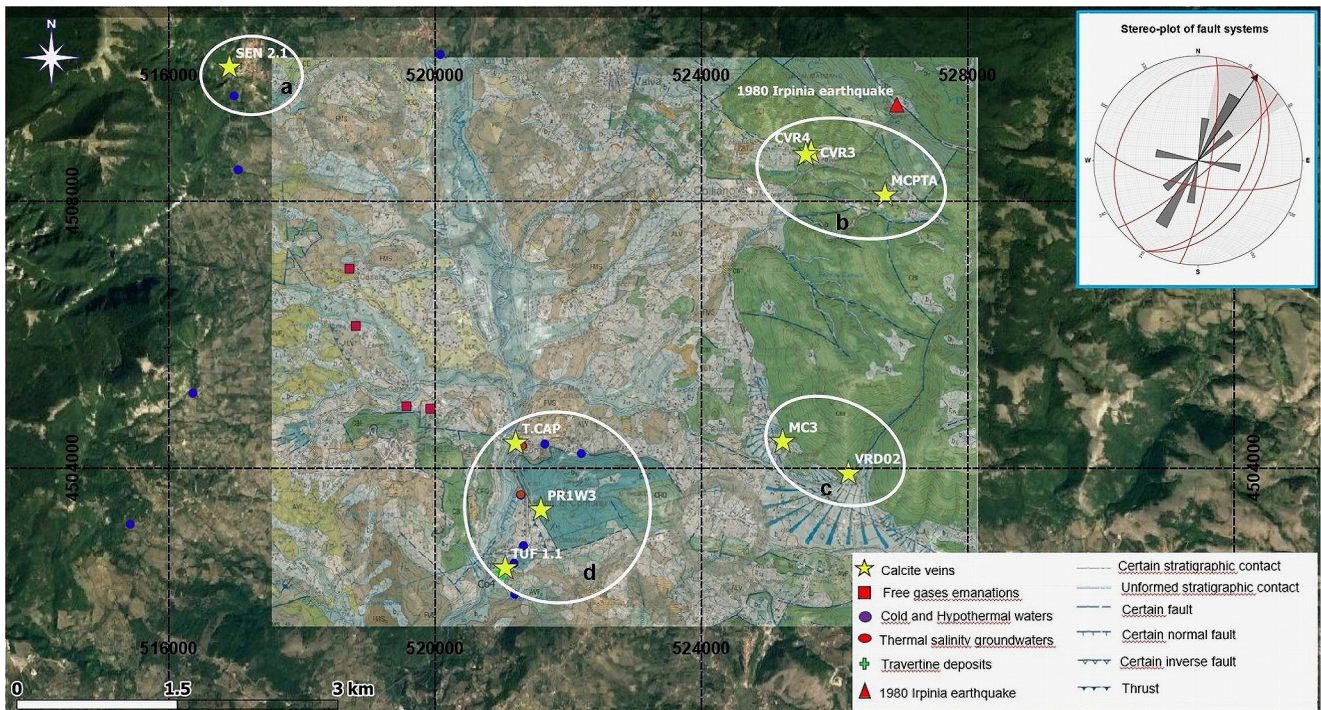


**Figure 2.** Detailed geological map (from CARG “CARTografia Geologica”) of the mineralization vein sampling sites (yellow stars) in the Irpinia region of southern Italy. Symbols: red squares, red triangles and blue circles indicate free gas emissions, hot saline thermal waters, and cold low-salinity waters, respectively (Buttitta et al., 2023; Gori et al., 2023); red triangle indicates 1980 Irpinia earthquake (Ciotoli et al., 2013). Insert shows a stereo plot of the two main medium—high angle fault sets identified in the study area.

took place by means of both thin-skinned and thick-skinned tectonics (Shiner et al., 2004), forming a complex multi-duplex that now day trending approximately N150° direction, subparallel to the strike direction of the main thrust faults (Patacca & Scandone, 2007). The tectono-stratigraphic units of the belt have been dissected by Plio-Quaternary high-angle faults associated with the aperture of the Tyrrhenian Sea and/or with the gravitational collapse of the contractional edifice (Vezzani et al., 2010). Extension currently occurs along the axial zone of the belt, whereas thrusting takes place along its frontal, peri-Adriatic sector.

Focusing on the axial zone of the southern Apennines, its uplifting began during the Middle to Upper Pleistocene and it became exhumed due to active extensional faults rooted at depths down to ca. 15 km, as suggested by surface and sub-surface geology, borehole breakout, and fault plane earthquakes. The greatest amount of stretching is in the NE–SW direction, with a computed extension rate of 3–5 mm/y (Ascione et al., 2013). In the study area, the main tectono-stratigraphic units of the belt consist of a deep-seated carbonate of the Apenninic Platform, and basinal rocks of the Lagonegro Basin (Patacca & Scandone, 2007). At the regional scale, low-angle thrust faults juxtapose the platform carbonates, at the hanging wall, against the Lagonegro units at the footwall. The entire accretionary wedge overrides the buried Apulian Platform (Figure 1a). The Contursi hydrothermal basin area is located along the Sele River valley. The structural setting of this area was previously interpreted as consisting of a N–S trending graben (Coppola & Pescatore, 1989) where, high-angle faults border the carbonate massifs and flank the Neogene-Quaternary continental deposits topping the Mesozoic carbonates (Figures 1a and 2).

### 3. Material and Methods

This study was performed using the following interdisciplinary approaches (a) 1:50,000-scale geological mapping using sheet (“468 Eboli”) map from CARG (CARTografia Geologica), (b) structural analyses of faults and fractures, (c) microstructural and textural analyses of calcite veins associated with the identified faults, (d) measurements of noble gases (He, Ne, and Ar concentrations and isotope ratios) in FIs within calcite veins, and (e) analyses of U and Th concentrations in calcite samples.

#### 3.1. Field Structural Analysis

Field measurements were made of the attitudes of the main fault planes, kinematic indicators such as striae and calcite steps, minor slip surfaces, barren fractures, and veins. Comb and slip-parallel veins are oriented perpendicular and parallel to the main fault planes, respectively (Hancock & Barka, 1987; Stewart & Hancock, 1990). These veins were initially interpreted as “tension cracks reflecting down-dip stretching during localized post-slip stress reorientation” (Hancock & Barka, 1987; Stewart & Hancock, 1990). However, it has more recently been proposed that comb and slip-parallel veins can also form during co-seismic down-dip displacement of the footwall block, and co-seismic stress release localizing the ingress and flow of deep over-pressured fluids (Smeraglia et al., 2018).

The comb and slip-parallel calcite veins analyzed in this study (10 samples, Table 1 and Figures in Supporting Information S1) were collected from an area that was approximately 40 km<sup>2</sup>-wide. The following four main sites were chosen (Figure 2): (a) Senerchia site (SEN 2.1 sample); (b) Colliano and Monte Carpineta fault sites (CVR3, CVR4, and MCPTA samples); (c) Monte Castello and Vallone Raio fault sites (MC3 and VRD02 respectively samples); (d) Contursi hydrothermal basin (T.CAP, PR1W3, and TUF 1.1 samples). These calcite veins cross-cut Lower Jurassic limestones, Upper Cretaceous dolomitic limestones, and Upper Paleogene marly limestones. The observed fault segments strike directions are either NW–SE or WNW–ESE. Only the TUF 1.1 calcite vein sample was not sampled near fault plane, but rather in a sinkhole structure with associated gas emissions. The sampled veins commonly include either whitish or greyish calcite crystals, with the latter ones probably associated with organic matter. Their widths range from a few millimeters up to about 1 cm. More details on the structural analysis in the field and the description of the samples are reported in Supporting Information S1.

#### 3.2. Microstructural Analyses and FIs Petrography

Microstructural analyses of calcite veins were performed by optical microscope on polished 40 to 50 μm-thick sections prepared at the University of Basilicata (Italy) and the University of Salamanca (Spain). Vein textures were described according to the following nomenclature reported by Bons et al. (2012): “blocky” was used to characterize roughly equidimensional and randomly oriented crystals, which implied rapid crack opening,



**Table 1**

General Data for Mineralization Vein Samples in Seismogenic Fault Systems in the Irpinia Region of Southern Italy

N°	Sample ID	Site	Typology	Latitude (N)	Longitude (E)
1	MC3_V1	Monte Castello (Contursi Terme)	Blocky calcite in comb-vein	40°41'24.37"	15°17'55.70"
2	MC3_V2	Monte Castello (Contursi Terme)	Fibrous calcite in comb-vein	40°41'24.37"	15°17'55.70"
3	VRD02	Vallone Raio (Contursi Terme)	Blocky calcite slip parallel vein	40°41'08.96"	15°18'35.48"
4	CVR3	Colliano Villa Rosa	Blocky calcite in comb vein	40°43'44.53"	15°18'13.63"
5	CVR4	Colliano Villa Rosa	Blocky calcite vein	40°43'44.53"	15°18'13.63"
6	PR1W3a PR1W3b	Monte Pruno (Contursi Terme)	Blocky calcite in comb-vein	40°40'51.03"	15°15'21.49"
7	TUF 1.1 TUF 1.1b	Terme Tufaro (Contursi Terme)	Blocky calcite vein	40°40'23.33"	15°14'56.21"
8	MCPTA	Monte Carpineta (Colliano)	Blocky calcite in comb vein	40°43'24.93"	15°19'01.95"
9	T.CAP	Terme Capasso (Contursi Terme)	Blocky calcite vein	40°41'24.05"	15°15'04.73"
10	SEN 2.1	Senerchia	Blocky calcite in comb and slip parallel veins	40°44'28.05"	15°12'01.50"

Note. Comb and slip-parallel veins are the nomenclature first proposed by Hancock and Barka (1987) and Stewart and Hancock (1990) according to the spatial relationships of veins with the fault plane. Blocky and fibrous calcite crystals are a texture proposed by Sibson (2000, 2012).

possibly mediated by fluid overpressure, and rapid precipitation in fluid-filled open cracks (Curzi et al., 2024); “fibrous” was used to characterize stretched or rod-shaped crystals, which showed a high length to width ratio. The latter textures were formed by progressive small increments of opening shearing and mineral precipitation (Gratier & Gamond, 1990; Passchier & Trouw, 2005).

FIs petrography was performed on doubly polished thin sections (60–80 μm thick) by using a Leica DM750P polarized optical microscope at 40x and 100x magnifications at the University of Salamanca, and a Zeiss Axiophot polarizing microscope hosted at the Laboratory of Fluid Inclusions of Sapienza- IGAG-CNR in Roma.

### 3.3. Analyses of Noble Gases in FIs

The noble gases (He, Ne and Ar concentrations and isotope ratios) in FIs trapped in calcite were analyzed at the noble gas laboratory of the Istituto Nazionale di Geofisica e Vulcanologia (INGV) in Palermo, Italy, following the preparation and analytical protocols described by Rizzo et al. (2018, 2021). After manually selecting calcite crystals (ca. 1 g for each sample) under a binocular microscope, the separated crystals were thoroughly cleaned in an ultrasonic bath in order to remove any impurities that remained attached to their surfaces. The washing process in the ultrasonic bath took 45 min and was carried out using Millipore water and acetone. Selected sample materials were loaded into a stainless-steel crusher and baked for 48–72 hr at 120°C in order to achieve ultra-high-vacuum conditions ( $10^{-9}$  mbar), using procedures described by Tantillo et al. (2009) in INGV Technical Reports. FIs from the minerals were released by an in-vacuum single-step crushing process, with an external pressure of 250 bar applied by a hydraulic press. This conservative procedure was used to minimize the contribution of cosmogenic  $^3\text{He}$  and radiogenic  $^4\text{He}$  that might have grown or been trapped in the crystal lattice (Rizzo et al., 2018 and references therein). Each session involved analyzing at least one standard sample for each of He, Ne and Ar with the standards corresponding to purified aliquots of air stored in a tank connected to a pipette with a calibrated volume. The air sample stored in the tank was originally collected close to the sea near Palermo and then cleaned using standard protocols in the preparation system at the INGV-noble gas laboratory in Palermo.

Noble gases were separated from the other volatiles by using a “cold finger” trap immersed in liquid nitrogen ( $temperature = -196^\circ\text{C}$ ) that allowed freezing of  $\text{H}_2\text{O}$  and  $\text{CO}_2$ , and were successively further cleaned in an ultra-high vacuum ( $10^{-9}$ – $10^{-10}$  mbar) purification line, with all species of the gas mixture other than noble gases being removed using four getters. He ( $^3\text{He}$  and  $^4\text{He}$ ) and Ne ( $^{20}\text{Ne}$ ) isotopes were measured separately using two different split-flight-tube mass spectrometers (Helix SFT-Thermo). The analytical uncertainty for all species in the gas mixture isotope ratio was  $\leq 4\%$ . The  $^{20}\text{Ne}$  isotope ratio was corrected for isobaric interferences at  $m/z$  values of 20 ( $^{40}\text{Ar}^{2+}$ ). Ar isotopes ( $^{36}\text{Ar}$ ,  $^{38}\text{Ar}$  and  $^{40}\text{Ar}$ ) were analyzed using a multicollector mass spectrometer

(GVI Argus) with an analytical uncertainty of 1.0%. The uncertainty in the determinations of the elemental contents of He, Ne, and Ar was <5%.

### 3.4. U–Th Concentrations in Calcite Veins

The concentrations of U and Th in bulk calcite veins and in two limestone host rocks were analyzed using inductively coupled plasma-mass spectrometry at the Actlabs research laboratories ([www.actlabs.com](http://www.actlabs.com)) with the WRA + Trace 4 Lithoresearch + 4B1 methodology. The detection limits for the U and Th concentrations were 0.01 and 0.05 ppm, respectively.

## 4. Results

### 4.1. Structural and Microstructural Results

Independent of the sampling sites, host-rock lithology and fault-strike directions, most of the studied calcite veins included blocky crystals (Figure S2 in Supporting Information S1). Despite the crosscutting relations and vein dip angles, the mineral precipitation post-dated the occurrence of brittle fracturing. This texture is commonly associated with precipitation in phreatic conditions, as recently documented by Manniello et al. (2023) and Todaro et al. (2024) for the Lower Jurassic carbonates exposed in the nearby area of Monte di Viggiano, and it can occur due to sealing of co-seismic fractures associated with transient fluid overpressure (Curzi et al., 2024). More details on the structural field analysis, faults and fractures direction, comb and slip parallel veins and calcite textures in the studied samples are reported in Supporting Information S1.

MC3 sample was the only one that also showed a probably syn-kinematic calcite and so for this reason, hereafter we focus on the results obtained in the detailed microstructural analyses conducted on this sample. This sample was collected along the Monte Castello fault (Figure S3 in Supporting Information S1), at a sub-vertical outcrop trending along the W–E direction and exposing Upper Cretaceous bio-lithoclastic limestone with rudists with a bedding attitude of N240°/20°N. The limestone rock was displaced by a small-scale fault with an attitude N30°/40°NW, and crosscut by a cleavage N270°/30°S. Furthermore, high-angle veins with an attitude of N170°/70°ENE (present within MC3 sample) cross-cut the hanging wall fault block (Figure S3 in Supporting Information S1). The microstructural analyses revealed three different calcite veins within MC3 sample, labeled as V1, V2, and V3 (Figure 3). Vein V1 consisted of a fractured blocky texture resulting from probably post-kinematic calcite minerals showing twinning at low angle with respect to the vein walls. Vein V2 was sub-parallel to vein V1 and included probably syn-kinematic fibrous calcite crystals oblique to the transverse vein walls. The tiny V3 vein was sub-parallel to the previous ones, and included blocky calcite crystals, and cross-cut the vein V2.

To sum up, the calcite veins cross-cut Lower Jurassic limestone, Upper Cretaceous dolomitic limestone rocks, and Upper Palaeogene. marly limestone. The observed fault segments strike directions were either NW–SE or WNW–ESE, and the calcite veins presented along two main strike directions: NNW–SSE and ENE–WSW. Most of the studied calcite veins included blocky crystals and in one case had a fibrous texture. More details are shown in Supporting Information S1.

### 4.2. Noble Gases Composition in FIs

FIs were arranged as small clusters within calcite grains (Figure 4). FIs contained a two-phase fluid (liquid and vapor) had a maximum size of 1–5  $\mu\text{m}$  with a volume fraction ( $\phi$ ) ranging between 10% and 20%. Figure 4 shows a representative Fluid Inclusion assemblage, that is, on petrographically discriminated, cogenic groups of FIs (Bodnar, 2003) found in vein V1 of MC3 sample. The MC3\_V2 mineralization vein is the only one displaying fibrous texture, which we interpreted as syn-kinematic structures. Here, FIs are arranged as small cluster and/or isolated inclusions in calcite crystals, suggesting their primary origin (Goldstein, 2003).

The calcite vein samples were analyzed to determine the concentrations and isotopic compositions of the light noble gases He, Ne, and Ar in FIs and also their isotope ratios ( $^3\text{He}/^4\text{He}$ ,  $^4\text{He}/^{20}\text{Ne}$  and  $^{40}\text{Ar}/^{36}\text{Ar}$ ) (Table 2).

The  $^4\text{He}$ ,  $^{20}\text{Ne}$  and  $^{40}\text{Ar}$  concentrations were  $8.80 \times 10^{-14}$ – $1.31 \times 10^{-11}$ ,  $1.39 \times 10^{-14}$ – $1.61 \times 10^{-13}$  and  $8.11 \times 10^{-12}$ – $9.84 \times 10^{-11}$  mol  $\text{g}^{-1}$ , respectively. The He isotope ratios ( $^3\text{He}/^4\text{He}$ ) were normalized to the value in air (where Ra is the atmospheric ratio of  $1.38 \times 10^{-6}$ ; Mabry et al., 2013), yielding values ranging from 0.08 Ra (TUF 1.1b sample) to 1.38 Ra (vein V2 in MC3 sample). The  $^4\text{He}/^{20}\text{Ne}$  ratios ranged from 1 (PR1W3a sample) to



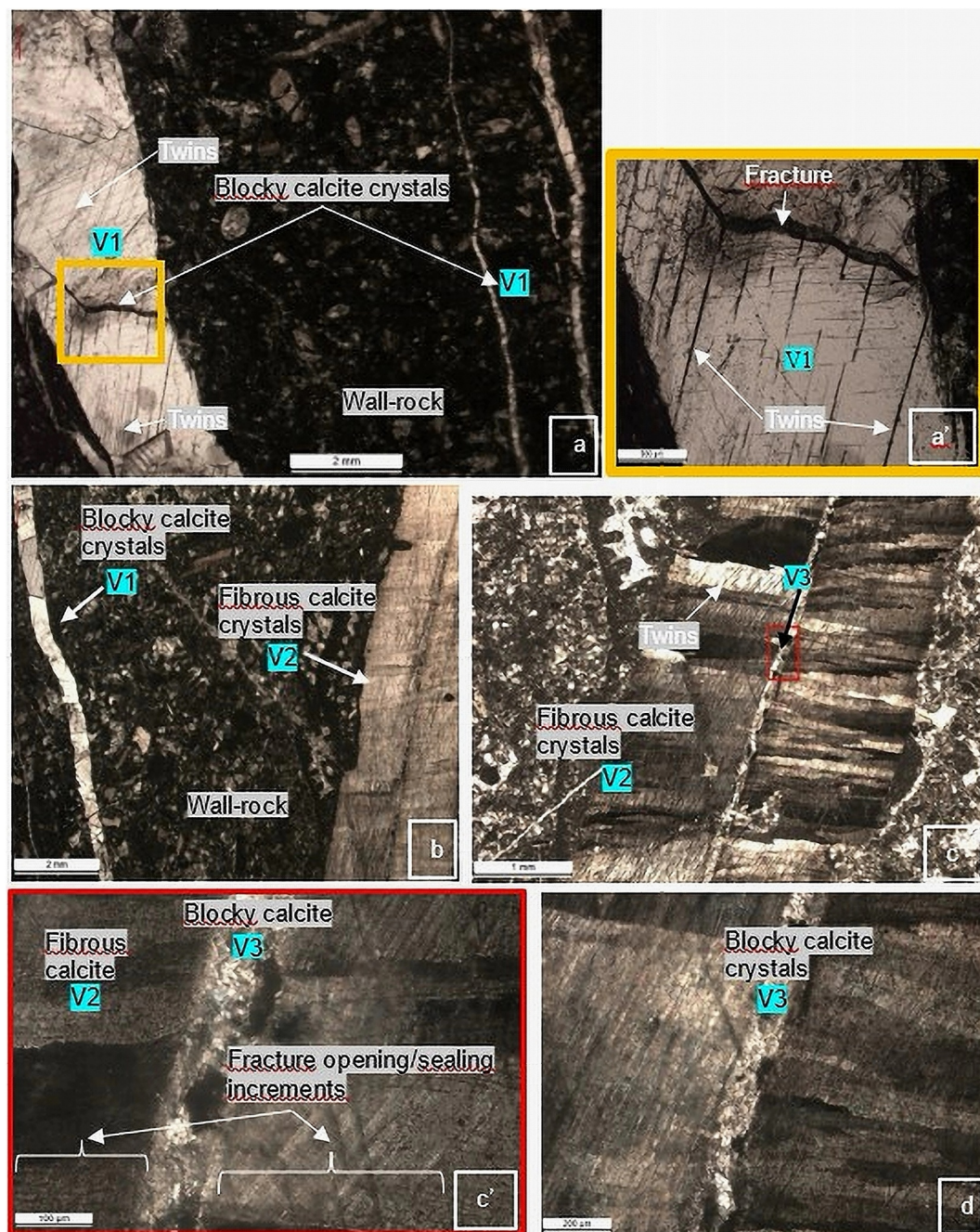


**Figure 3.** Microstructural analyses of the sample MC3 fault-related mineralizations taken from the thigh in section observed under an optical microscope by cross-polarized light. (a, a') Blocky calcite crystal with a high angle comb-vein mineralization; (b) Blocky calcite crystals (V1), post-kinematic, associated with a V2 fibrous calcite vein, syn-kinematic; (c, c', d) Fibrous calcite vein, syn-kinematic (V2) associated with a vein with small blocky calcite crystals post-kinematic (V3), and with fracture opening/sealing increment.

81.7 (TUF 1.1 sample). These values were higher than those found in both atmosphere and air-saturated water (ASW), at 0.319 and 0.285, respectively, at 25°C (Ozima & Podosek, 2002). The  $^{40}\text{Ar}/^{36}\text{Ar}$  ratio varied from 302.2 (CVR3 sample) to 404.6 (vein V2 in MC3 sample), and hence was slightly higher than that in the atmosphere (298.6; Lee et al., 2006), which is consistent with an excess of no atmosphere-derived  $^{40}\text{Ar}$ . We computed the concentration of deep-sourced  $^{40}\text{Ar}$  (due to  $^{40}\text{K}$  decay in the mantle and/or in the crust) using the following equation reported by Graham (2002):

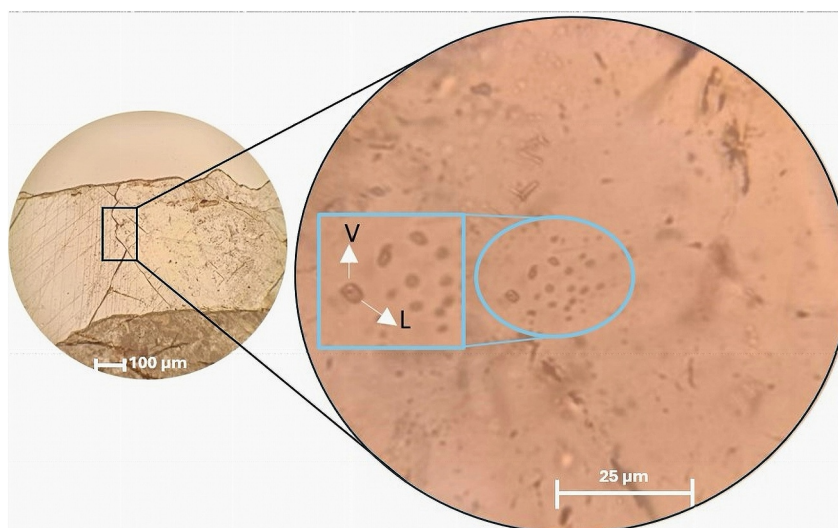


**Figure 4.** Representative textural distribution (parallel polars) of fluid inclusions trapped in calcite veins (sample MC3\_V1) from optical microscopy analyses. L = liquid; V = vapor.

$$^{40}\text{Ar}^* \approx \left[ (^{40}\text{Ar}/^{36}\text{Ar})_{\text{sample}} * (^{36}\text{Ar})_{\text{sample}} \right] - \left[ (^{40}\text{Ar}/^{36}\text{Ar})_{\text{air}} * (^{36}\text{Ar})_{\text{sample}} \right] \quad (1)$$

where  $(^{40}\text{Ar}/^{36}\text{Ar})_{\text{sample}}$  and  $(^{36}\text{Ar})_{\text{sample}}$  are the measured values, and  $(^{40}\text{Ar}/^{36}\text{Ar})_{\text{air}}$  is the aforementioned isotopic value in atmosphere (298.6; Lee et al., 2006). The computed  $^{40}\text{Ar}^*$  concentration ranged from  $2.76 \times 10^{-13}$  to  $6.04 \times 10^{-12}$  mol g<sup>-1</sup>, while the  $^{40}\text{Ar}^*/^4\text{He}$  ratio varied from 0.19 to 36.74.

Considering that  $^3\text{He}$  was  $1.17 \times 10^{-18}$  to  $1.49 \times 10^{-18}$  mol g<sup>-1</sup>,  $^4\text{He}$  was  $7.81 \times 10^{-13}$  to  $7.77 \times 10^{-13}$  mol g<sup>-1</sup>,  $^{40}\text{Ar}/^{36}\text{Ar}$  was 316.3–404.6 and  $^{40}\text{Ar}^*$  was  $1.91 \times 10^{-12}$  to  $7.38 \times 10^{-12}$  mol g<sup>-1</sup> at the Monte Castello fault site, a marked difference was found between post-kinematic blocky calcite (vein V1 in MC3 sample) and syn-kinematic fibrous calcite (vein V2 in MC3 sample) in terms of both R/Ra (where R is the He isotopic signature of the sample) and  $^{40}\text{Ar}/^{36}\text{Ar}$  (Table 2). Vein V2 (1.38 Ra,  $^{40}\text{Ar}/^{36}\text{Ar} = 404.6$  and  $^{40}\text{Ar}^* = 1.91 \times 10^{-12}$  mol g<sup>-1</sup>) exhibited higher values than vein V1 (1.07 Ra,  $^{40}\text{Ar}/^{36}\text{Ar} = 316.3$  and  $^{40}\text{Ar}^* = 7.38 \times 10^{-12}$  mol g<sup>-1</sup>), indicating a mantle He component.

### 4.3. U and Th Bulk Analysis

The calcite vein samples were also analyzed to determine the U and Th concentrations; the results are presented in Table 3. The U and Th concentrations ranged from 0.1 to 1 ppm and from 0.1 to 0.2 ppm, respectively. These ranges are consistent with the U and Th concentrations of calcites worldwide being around 1 ppm (Coltorti et al., 2011 and reference therein). Samples MC3\_V1 and T.CAP had Th concentrations lower than the detection limit of 0.05 ppm.

## 5. Discussion

### 5.1. Fluid Sources

The primary sources of fluids are in the mantle, crust and atmosphere. Since noble gases are not reactive, the origin of He in natural fluids can be traced by using their isotopic signature (e.g., Ozima & Podosek, 2002). A useful approach for discriminating the He origin is to obtain the values for three possible endmembers by using binary mixing equations (Figure 5a) combining the He isotopic ratios (R/Ra) and the  $^4\text{He}/^{20}\text{Ne}$  ratios of the three endmembers (Sano et al., 1987). Specifically, here we assume a mantle endmember as the Sub Continental Lithospheric Mantle (SCLM) whose R/Ra is  $6.32 \pm 0.39$  (mean  $\pm$  SD) and  $^4\text{He}/^{20}\text{Ne} > 1,000$  (Gautheron et al., 2005; Sano & Marty, 1995). The crustal and the atmospheric endmembers have an R/Ra of 0.02 and



**Table 2**  
*Chemical Compositions of Noble Gases (He, Ne, and Ar) and Their Isotopic Ratios in Fluid Inclusions Trapped in Calcite Veins Associated With Seismogenic Faults*

Sample ID	<sup>4</sup> He mol/g	<sup>4</sup> He error	<sup>3</sup> He mol/g	<sup>3</sup> He error	<sup>20</sup> Ne mol/g	<sup>20</sup> Ne error	<sup>40</sup> Ar mol/g	<sup>40</sup> Ar error	<sup>4</sup> He/ <sup>20</sup> Ne
PR1W3a	8.80E−14	0.10	7.84E−20	20.02	8.44E−14	0.90	4.13E−11	0.09	1.0
PR1W3b	1.72E−13	0.09	1.91E−19	19.09	8.99E−14	0.59	4.29E−11	0.11	1.9
VRD02	7.16E−13	0.12	7.06E−19	5.42	5.61E−14	1.00	3.43E−11	0.10	12.8
MC3_V1	7.81E−13	0.03	1.17E−18	4.20	7.00E−14	0.60	3.07E−11	0.13	11.2
CVR3	2.73E−13	0.03	4.13E−19	5.90	1.39E−14	0.66	8.11E−12	0.07	19.6
CVR4	1.96E−12	0.02	2.92E−18	2.45	4.34E−14	0.94	1.74E−11	0.07	45.3
MC3_V2	7.77E−13	0.02	1.49E−18	2.97	5.52E−14	0.51	2.77E−11	0.06	14.1
MCPTA	8.18E−13	0.03	8.41E−19	3.60	2.34E−14	0.52	2.06E−11	0.06	34.9
T.CAP	2.84E−12	0.02	2.09E−18	2.86	4.27E−14	0.46	3.03E−11	0.11	66.5
TUF 1.1	1.31E−11	0.02	2.05E−18	3.02	1.61E−13	0.63	9.43E−11	0.06	81.7
TUF 1.1b	1.28E−11	0.02	1.56E−18	3.02	1.72E−13	0.67	9.84E−11	0.07	74.4
SEN 2.1	1.09E−12	0.02	8.48E−19	3.91	2.48E−14	0.50	1.62E−11	0.06	44.0

Sample Id	R/Ra	Total error ±	<sup>40</sup> Ar/ <sup>36</sup> Ar	Error (%)
PR1W3a	0.64	0.13	321.8	0.21
PR1W3b	0.80	0.15	318.3	0.24
VRD02	0.71	0.04	315.8	0.18
MC3_V1	1.07	0.05	316.3	0.32
CVR3	1.09	0.06	307.0	0.05
CVR4	1.07	0.03	303.1	0.06
MC3_V2	1.38	0.04	404.6	0.04
MCPTA	0.74	0.03	383.3	0.04
T.CAP	0.53	0.02	315.6	0.02
TUF 1.1	0.11	0.00	320.6	0.01
TUF 1.1b	0.09	0.00	316.0	0.01
SEN 2.1	0.56	0.02	303.2	0.05

Note. Note: unit of error is in %.

**Table 3**  
*Concentrations of U and Th From Calcite Veins, Expressed in ppm*

Sample ID	[U] <sub>ppm</sub>	[Th] <sub>ppm</sub>
T.CAP	0.9	b. d. l
PRW3a	0.8	0.2
MC3_V1	0.1	b. d. l
VRD02	1.0	0.1
CVR3	0.2	0.1
T.CAPH	2.18	0.06
CVRH	0.12	0.06

Note. T.CAPH and CVRH are limestone host rock respectively. b. d. l., below detection limit. Detection limits for [U] and [Th] were 0.01 and 0.05, respectively.

<sup>4</sup>He/<sup>20</sup>Ne > 1,000 (Sano & Marty, 1995), for atmosphere (air) R/Ra is 1, and <sup>4</sup>He/<sup>20</sup>Ne is 0.319 (Ozima & Podosek, 2002) and ASW has an R/Ra of 1 and <sup>4</sup>He/<sup>20</sup>Ne = 0.285 at 25°C (Ozima & Podosek, 2002).

Most of the investigated samples show <sup>4</sup>He/<sup>20</sup>Ne values two-three orders of magnitude higher than in atmosphere, which is consistent with a negligible amount of atmospheric He. Both samples PR1W3a and PR1W3b are characterized by the low <sup>4</sup>He/<sup>20</sup>Ne ratios of 1.0 and 1.9, respectively, and a He isotopic signature ranging from 0.64 to 0.80 Ra, and hence the atmospheric He component could mask the original paleofluid signature. Figure 5a shows two different clusters of He isotope ratio. The first cluster is between 0.53 and 1.38 Ra, consistent with a 10%–20% of the mantle-derived He (considering an SCLM) and 80%–90% coming from the crust. The second cluster pertaining to samples TUF1.1a and TUF 1.1b collected from the Tufaro thermal area shows relatively pure crustal-derived He with negligible amounts of atmospheric and mantle He. We note that the strongest measured He isotopic signature in FIs (1.38 Ra, MC3\_V2 sample) fits well with data pertaining to the presence of high-flux CO<sub>2</sub> gas emission in the area (Buttitta et al., 2023;

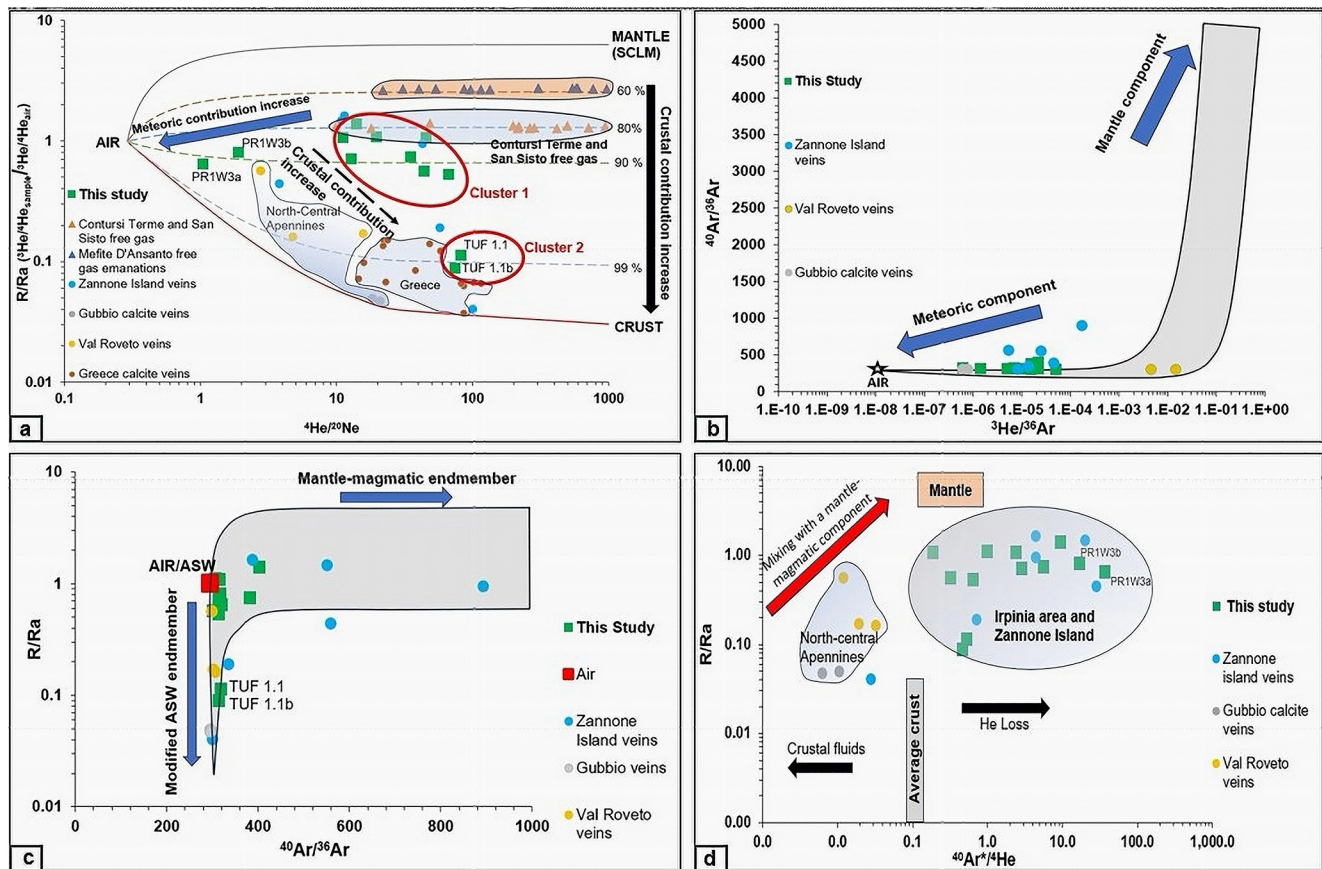


**Figure 5.** (a) Diagram of the correlation between the  $^3\text{He}/^4\text{He}$  and  $^4\text{He}/^{20}\text{Ne}$  ratios for the fluid inclusions (FIs) in calcite veins. Solid lines depict binary mixing between air ( $^3\text{He}/^4\text{He} = 1 \text{ Ra}$ ,  $^4\text{He}/^{20}\text{Ne} = 0.319$ ; Ozima & Podosek, 2002), the Sub Continental Lithospheric Mantle ( $^3\text{He}/^4\text{He} = 6.32 \pm 0.39 \text{ Ra}$ , Gautheron et al., 2005;  $^4\text{He}/^{20}\text{Ne} > 1,000$ , Sano & Marty, 1995), crustal endmember ( $^3\text{He}/^4\text{He} = 0.01\text{--}0.05 \text{ Ra}$ ,  $^4\text{He}/^{20}\text{Ne} > 1,000$ ; Sano & Marty, 1995). Reference data: Contursi free gas data (Buttitta et al., 2023; Caracausi & Paternoster, 2015), Zannone island veins (Curzi et al., 2022), Gubbio calcite veins (Marchesini et al., 2022), Val Roveto veins (Smeraglia et al., 2018), Mefite D'Ansanto free gas (Caracausi & Paternoster, 2015), and calcite fault zone in Greece (Pik & Marty, 2009). (b) Plot of  $^3\text{He}/^{36}\text{Ar}$  versus  $^{40}\text{Ar}/^{36}\text{Ar}$ . The gray region is consistent with mixing between mantle-magmatic fluids that are enriched in  $^{40}\text{Ar}$  and  $^3\text{He}$  and a fluid with air or air-saturated water (ASW) black star:  $^3\text{He}/^{36}\text{Ar} = 1 \times 10^{-8}$  and  $^{40}\text{Ar}/^{36}\text{Ar} = 296.6$ ; Kendrick & Burnard, 2013). The gray shading indicates literature data that are representative of mixing (Kendrick & Burnard, 2013 and references therein; Goodwin et al., 2017; Tang et al., 2017; Wu et al., 2018). (c) Schematic of He and Ar isotopes of FIs in calcite. The gray shading indicates data from previous investigations of FIs with both magmatic and crustal origins in various worldwide ore deposits (literature data in Figure 6b). The red rectangle represents the air and ASW endmember. The modified air endmember is ASW that is simply enriched by the addition of radiogenic  $^4\text{He}$  (Kendrick & Burnard, 2013 and reference therein). (d) Plot of  $^{40}\text{Ar}^*/^4\text{He}$  versus  $^3\text{He}/^4\text{He}$  (as R/Ra). The compositions of the following two fields are from Kendrick and Burnard (2013): (1) average crust, (2) mantle. Red arrow shading indicate mixing between the crustal and mantle-magmatic fluids.

Caracausi & Paternoster, 2015; Figure 5a). This similarity indicates that the ratio of crust-to-mantle He in FIs remained approximately constant over time along the studied faults. The age of the calcite veins is still unknown, and it could provide new constrains on the timing of mantle He degassing in this area of southern Italy.

### 5.2. Fault-Controlled He Flow and/or Vein Aging

The large variability of He isotopic signature documented for the studied FIs ( $R/Ra = 0.09\text{--}1.38$ ) is not consistent with that documented for the current outgassing that characterizes the study area (Figure 5a), which show a narrower range of values ( $R/Ra = 1.27\text{--}1.41$ ,  $^4\text{He}/^{20}\text{Ne} > 3$ ; Buttitta et al., 2023 and reference therein). In fact, we note that 20 years of low-frequency geochemical monitoring of the Contursi hydrothermal basin has revealed a 0.2 Ra variability of the He isotopic signature of the currently outgassing fluids (Buttitta et al., 2023 and reference therein). During this time span, the background seismicity of the area recorded seismic events with magnitudes  $M_w < 4$  (<http://isnet-bulletin.fisica.unina.it/cgi-bin/isnet-events/isnet.cgi>). This means that the background seismicity has not induced any short-term variation in the He isotopic signature (Caracausi et al., 2022 and reference therein).

**Table 4**

*<sup>4</sup>He Production Over Different Times Assumed That the U and Th Concentrations Were Close to 1 ppm in Calcite (Ballantine & Burnard, 2002)*

<sup>4</sup> He, atoms g <sup>-1</sup> year <sup>-1</sup>	Years	<sup>4</sup> He, mol/g year <sup>-1</sup>
4.01 × 10 <sup>6</sup>	1	6.66 × 10 <sup>-18</sup>
	10	6.66 × 10 <sup>-17</sup>
	10 <sup>2</sup>	6.66 × 10 <sup>-16</sup>
	10 <sup>3</sup>	6.66 × 10 <sup>-15</sup>
	10 <sup>4</sup>	6.66 × 10 <sup>-14</sup>
	10 <sup>5</sup>	6.66 × 10 <sup>-13</sup>
	10 <sup>6</sup>	6.66 × 10 <sup>-12</sup>
	10 <sup>7</sup>	6.66 × 10 <sup>-11</sup>

Considering that all studied veins are made up of calcite minerals (cf. Figures S1 and S2 in Supporting Information S1), and that the concentrations of both U and Th are ≤ 1 ppm (Table 3), we propose a twofold explanation for the variability of the He isotopic signature in FIs. We invoke a “early trapping processes” enhanced by rock fracturing potentially during earthquakes, which increased the amount of crustal <sup>4</sup>He within the circulating paleofluids (Caracausi et al., 2022), and a “post-trapping processes” due to the addition of radiogenic He produced within veins over time (vein aging). The “early trapping” hypothesis suggests that the mineralizing fault fluids captured the <sup>4</sup>He released by the fractured and fragmented host rocks due to localized dilatancy of these rocks (Caracausi et al., 2022). This dilatancy could occur during the preparatory phase of main earthquakes (foreshock events), which produces the release of crustal <sup>4</sup>He (Bauer et al., 2016; Honda et al., 1982) into the atmosphere because of volumetric stress changes (Ballantine & Burnard, 2002; Caracausi et al., 2022). The “post-trapping” hypothesis is

based on the production of <sup>4</sup>He by the decay of U and Th within the calcite minerals, and on its successive migration toward the FIs (Ballantine & Burnard, 2002). Nevertheless, these data are consistent with other studies on FIs trapped in calcite travertine samples for the fault zones exposed in western and Northern Turkey (Rizzo et al., 2019).

The first working hypothesis (i.e., early trapping) is supported by as the high degree of fracturing documented for the studied calcite veins (cf. Figure 3 and Figure S2 in Supporting Information S1). If so, the pronounced release of <sup>4</sup>He from the fault-related fractured and fragmented rock volumes can be associated with the main shocks that occurred in the studied area (Bello et al., 2021), and therefore with many previous high-magnitude earthquakes (Mw > 6) that have devastated the study area (Bello et al., 2021), and consequently to the direct link between seismicity and the impulsive nature of crustal <sup>4</sup>He degassing (Buttitta et al., 2020). Such a linkage has been already documented by the increase of crustal <sup>4</sup>He in natural fluids during strong earthquakes such as the Mw = 7.3 (2016 Kumamoto earthquake, Japan), and the Mw = 7.2 (1995 Kobe earthquake, Japan) (Sano et al., 1998, 2016). Accordingly, the pre-trapping hypothesis is supported by the high He isotopic variability recorded in the studied FIs (cf. Figure 5) and can be associated with main seismic events such as the aforementioned 1995 Kobe earthquake characterized by 1 Ra variation of the He isotopic signature in close groundwaters. Such a 1 Ra variation of the He isotopic signature coincides with the values that we documented for the Contursi hydrothermal basin (R/Ra = 0.09–1.38) with an absolute concentration of <sup>4</sup>He ranging from a minimum of 7.77 × 10<sup>-13</sup> mol/g (sample MC3\_V2, phase of the probable seismic activity or immediately after) up to a maximum of 1.31 × 10<sup>-11</sup> mol/g (sample TUF1.1), excluding the PR1W3a sample (Table 2).

Considering the post-trapping hypothesis, the following equation is employed to calculate the production of <sup>4</sup>He (Ballantine & Burnard, 2002):

$${}^4\text{He atoms g}^{-1}\text{yr}^{-1} = (3.115 \times 10^6 + 1.272 \times 10^5)[\text{U}] + 7.710 \times 10^5[\text{Th}] \quad (2)$$

where [U] and [Th] are the U and Th concentrations, respectively, which in this study we assumed were both close 1 ppm (Coltorti et al., 2011; Torgersen, 2010). To interpret the He isotopic signature of the studied Contursi FIs (cf. cluster 1 in Figure 5a) showing a mantle component (from 0.53 to 1.38 Ra), we compute the amount of He produced from 1 g of calcite, which is approximately 6.66 × 10<sup>-18</sup> mol/yr (See Table 4). We therefore conclude that <sup>4</sup>He produced from calcite at 0.1 Ma has been totally transferred to the FIs. We note that the Tufaro Terme samples (TUF 1.1 and TUF 1.1b) exhibited a dominant <sup>4</sup>He component (R/Ra = 0.09–0.11), similar to those measured in calcite veins of the northern-central Apennines of Italy (Marchesini et al., 2022; Smeraglia et al., 2018), and Greece (Pik & Marty, 2009). The latter data could hence result from the occurrence of both post and early trapping processes over different time periods (Figure 5 and Table S1 in Supporting Information S1).

### 5.3. Mixing of Deep and Meteoric-Derived Fluids

The signature of atmospheric fluids was assessed for the studied calcite veins by also considering the Ar isotopes (cf. Table 2). Since both <sup>3</sup>He and <sup>36</sup>Ar are not radiogenic, and their ratio in pure ASW is 5 × 10<sup>-8</sup> (Kendrick &



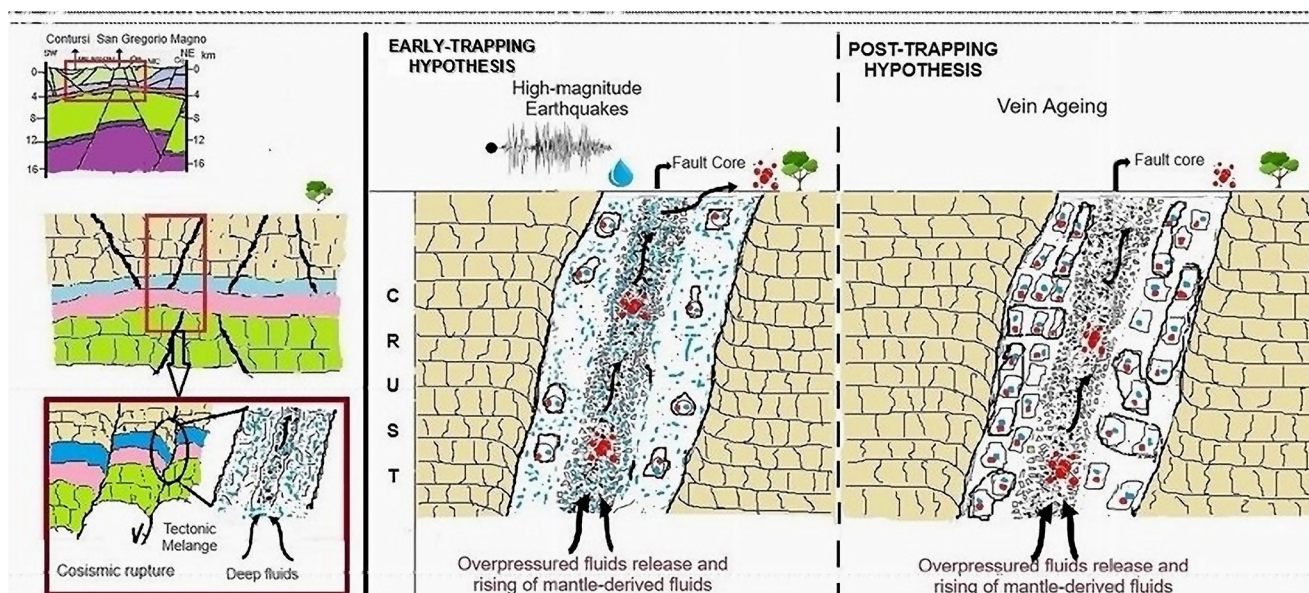


**Figure 6.** Simplified models for the early trapping hypothesis enhanced by rock fracturing potentially during earthquakes, which increased the amount of crustal  $^4\text{He}$  within the circulating paleofluids; for the post-trapping hypothesis have addition of radiogenic He produced within veins over time (vein ageing).

Burnard, 2013 and references therein), the  $^3\text{He}/^{36}\text{Ar}$  and  $^{40}\text{Ar}/^{36}\text{Ar}$  ratios documented for the Contursi FIs can help in identifying possible atmospheric inputs. Although the  $^{40}\text{Ar}/^{36}\text{Ar}$  ratios (up to 404, Table 2) were close to the atmosphere signature (298.6; Lee et al., 2006), their  $^3\text{He}/^{36}\text{Ar}$  ratios were up to three orders of magnitude higher than in the atmosphere (Kendrick & Burnard, 2013). Combining the two aforementioned ratios,  $^3\text{He}/^{36}\text{Ar}$  versus  $^{40}\text{Ar}/^{36}\text{Ar}$  (Figure 5b), we assess that an atmosphere-derived component was mixed with deeper sourced components. This interpretation is supported by the relation between R/Ra and  $^{40}\text{Ar}/^{36}\text{Ar}$  (Figure 5c), which shows that the fluids trapped in FIs included an atmospheric component mixed with fluids characterized by a dominant crustal component. Such an interpretation agrees with the data produced by Curzi et al. (2022) for the high-angle fault zones of the Zannone Island, along the Tyrrhenian coastline of Italy.

In contrast, the TUF samples showed a dominant crustal component with modified ASW end-members, referring to fluids that partially preserved the ASW signature but were modified during crustal residence (Kendrick & Burnard, 2013 and references therein). In fact, the He isotope system is more likely modifiable than heavier noble gases due to the very low abundance of He isotopes in ASW. Finally, in absence of a preferential He leakage by diffusion and advection, the ratio between radiogenic crustal  $^4\text{He}$  and  $^{40}\text{Ar}^*$  is expected to be like the crustal production ( $^{40}\text{Ar}^*/^4\text{He} \sim 0.1\text{--}0.2$ ; Kendrick & Burnard, 2013). Alternatively, the  $^{40}\text{Ar}^*/^4\text{He}$  can derive from mantle production ( $^{40}\text{Ar}^*/^4\text{He} \sim 0.1\text{--}1$ ; Curzi et al., 2022 and references therein). Considering the original data obtained for the study area (Figure 5d), with the calcite veins showing higher values of the  $^4\text{He}/^{40}\text{Ar}$  ratio with respect to the crustal production (cf. Section 4.2), we conclude that a significant mantle contribution is present in the study FIs. It is therefore possible to hypothesize that significant crustal-derived He loss does not affect the isotopic composition of the same elements (e.g.,  $^3\text{He}/^4\text{He}$  and  $^{40}\text{Ar}/^{36}\text{Ar}$ ).

## 6. Conclusions

Noble gases information within FIs trapped in calcite veins along seismogenic faults of Contursi hydrothermal basin (Irpina, southern Italy) provides, a better understanding of the fluids origin and circulation paths through fault zones, and their possible relations with past seismic activity, or vein aging (Figure 6, early and post trapping hypothesis). The study area is characterized by water temperature in the range of 26–47°C a currently background seismicity of  $M_w < 4$  and mantle-derived He outgassing. We combined field and microstructural analyses of fault-related calcite veins with noble gases (He, Ne, Ar concentration and their isotopic ratios) analyses in FIs within calcite veins.

The results showed that the fault-related calcite veins from the Contursi hydrothermal basin have a comb-veins and are characterized by a blocky calcite texture, and we interpreted this as potential for post-kinematics mineralization. Only one of the studied samples exhibited a fibrous calcite texture, potentially related to syn-kinematic mineralization.

Most of the Contursi FIs are characterized by a noble gases isotopic signature (He, Ne and Ar) consistent with the mixing of volatiles derived from both crustal and mantle sources. The variability of the He isotopic signature in the FIs (three of 10 FIs are out of the mixing trend) can be due to early trapping processes (probably earthquakes occurred in the past) or to post-trapping processes. The latter (vein aging) favors the production of  $^4\text{He}$  due to U and Th decay within the calcite and on its successive migration toward the FIs.

Regarding the outliers, sample PR1W3 showed an atmospheric component possibly masking the original He signature, sample TUF1.1 displayed a very negligible mantle contribution and a dominant crustal contribution, and sample MC3\_V2 shown the highest He isotopic signature in the FIs (1.38 Ra). The latter value fits well with the 1.41Ra of the currently high flux  $\text{CO}_2$  gaseous emission, indicating that the pristine mantle contribution did not vary over time. The latest He isotope values revealed mantle contribution up to 20% of the total He component.

Our conclusions are in line with previous studies describing mantle-derived fluids uprise along deep-rooted faults and/or outgassed from magmatic intrusions. The plausible temporal formation of the calcite veins suggests that the pristine mantle source has been active in the area for, at least, the last 1 Ma, corresponding to the active extensional tectonic age that characterizes the Contursi hydrothermal system. Ongoing analysis aiming at assessing carbon and oxygen stable isotopes of the calcite veins, and the petrographic, microthermometry and Raman of FIs should complement the knowledge of the mechanisms of fluid circulation from deep-seated sources, and their possible mixing with meteoric derived fluids during the long-term activity of general worldwide fault zones and the Contursi basin ones in particular.

## Data Availability Statement

All Supporting Figure and Tables are uploaded as part of the Supporting Information S1 to this article for review purposes. The complete data in Table S1 in Supporting Information S1 for plotting Figure 5 in main text, in addition to our unpublished data on the noble gases of FIs on calcite veins in the Contursi Basin, are available from: Ozima and Podosek (2002), Gautheron et al. (2005); Sano and Marty (1995); Buttitta et al. (2023); Caracausi and Paternoster (2015); Curzi et al. (2022); Marchesini et al. (2022); Smeraglia et al. (2018); Caracausi and Paternoster (2015); and calcite fault zone in Pik and Marty (2009); Kendrick and Burnard (2013); Tang et al. (2017); Goodwin et al. (2017); Wu et al. (2018).

## Equations Captions

Eq. 1: Equation for concentration of radiogenic Ar derived from the mantle, denoted  $40\text{Ar}^*$  by Graham (2002).

Eq. 2: Equation for the number of atoms of  $^4\text{He}$  produced in 1 g of rock per year (Ballantine & Burnard, 2002).

## References

- Agosta, F., Alessandrini, M., Tondi, E., & Aydin, A. (2009). Oblique normal faulting along the northern edge of the Majella Anticline, central Italy: Inferences on hydrocarbon migration and accumulation. *Journal of Structural Geology*, 32(9), 1327–1333. <https://doi.org/10.1016/j.jsg.2010.10.007>
- Agosta, F., & Kirschner, D. L. (2003). Fluid conduits in carbonate-hosted seismogenic normal fault of central Italy. *Journal of Geophysical Research*, 108, B4–2221. <https://doi.org/10.1029/2002JB002013>
- Amoroso, O., Ascione, A., Mazzoli, S., Virieux, J., & Zollo, A. (2014). Seismic imaging of a fluid storage in the actively extending Apennine Mountain belt, southern Italy. *Geophysical Research Letters*, 41(11), 3802–3809. <https://doi.org/10.1002/2014GL060070>
- Amoroso, O., Russo, G., De Landro, G., Zollo, A., Garambois, S., Mazzoli, S., et al. (2017). From velocity and attenuation tomography to rock physical modeling: Inferences on fluid-driven earthquake processes at the Irpinia fault system in southern Italy. *Geophysical Research Letters*, 44(13), 6752–6760. <https://doi.org/10.1002/2016GL072346>
- Ascione, A., Mazzoli, S., Petrosino, P., & Valenti, E. (2013). A decoupled kinematic model for active normal faults: Insights from the 1980, MS = 6.9 Irpinia earthquake, southern Italy. *Geological Society of America Bulletin*, 125(7/8), 1239–1259. <https://doi.org/10.1130/B30814.1>
- Ballantine, C. J., & Burnard, P. G. (2002). Production, Release, and transport of noble gases in the continental crust. *Reviews in Mineralogy and Geochemistry*, 47(1), 481–538. <https://doi.org/10.2138/rmg.2002.47.12>
- Balsamo, F., Clemenzi, L., Storti, F., Mozafari, M., Solum, J., Swennen, R., et al. (2016). Anatomy and Paleofluids evolution of laterally restricted extensional fault zones in the Jabal Qusaybah anticline, Salakh arch, Oman. *The Geological Society of America*, 128(5–6), 957–972. <https://doi.org/10.1130/B31317.1>

## Acknowledgments

This research was carried out in the frame of the national project PRINFLUIDS (Grant 20174X3P29\_005) and the national PON GRINT (Geoscience Research Infrastructure in Italy) CCI:2014IT16M2OP005. Antonio Caracausi appreciates support by the “Ramón y Cajal” research program (RYC2021-033270-I; MCIN/AEI/10.13039/501100011033—EU “NextGenerationEU/PRTR”). A.M.A.-V thanks the assistance of the research project ERUPTING (PID2021-127189OB-I00) funded by MCIN/AEI/10.13039/501100011033. Open access publishing facilitated by Università degli Studi della Basilicata, as part of the Wiley - CRUI-CARE agreement.

- Bauer, S. J., Gardner, W. P., & Heath, J. E. (2016). Helium release during shale deformation: Experimental validation. *Geochemistry, Geophysics, Geosystems*, 17(7), 2612–2622. <https://doi.org/10.1002/2016GC006352>
- Bello, S., De Nardis, R., Scarpa, R., Bozzetti, F., Cirillo, D., Ferrarini, F., et al. (2021). Fault Pattern and seismotectonic style of the Campania-Lucania 1980 earthquake (Mw 6.9, southern Italy): New multidisciplinary constrains. *Frontier in Earth Science*, 8. <https://doi.org/10.3389/feart.2020.608063>
- Bernard, P., & Zollo, A. (1989). The Irpinia (Italy) 1980 earthquake: Detailed analysis of a complex normal faulting. *Journal of Geophysical Research*, 94(B2), 1631–1647. <https://doi.org/10.1029/JB094iB02p01631>
- Bodnar, R. J. (2003). Reequilibration of fluid inclusions. In I. Samson, A. Anderson, & D. Marshall (Eds.), *Fluid inclusions: Analysis and interpretation*. Mineral. Assoc. Canada, short course (Vol. 32, pp. 213–230).
- Boles, J. R., Garven, G., Camacho, H., & Lupton, J. E. (2015). Mantle helium along the Newport-Inglewood fault zone. *Geochemistry, Geophysics, Geosystems*, 16(7), 2364–2381. <https://doi.org/10.1002/2015GC005951>
- Bons, P. D., Elburg, M. A., & Rivas, E. G. (2012). A review of the formation of the tectonic veins and their microstructures. *Journal of Structural Geology*, 43, 33–62. <https://doi.org/10.1016/j.jsg.2012.07.005>
- Buttitta, D., Capasso, G., Paternoster, M., Barberio, M. D., Gori, F., Petitta, M., et al. (2023). Regulation of deep carbon degassing by gas-rock-water interactions in a seismic region of Southern Italy. *Science of the Total Environment*, 897, 165367. <https://doi.org/10.1016/j.scitotenv.2023.165367>
- Buttitta, D., Caracausi, A., Chiaraluce, L., Favara, R., Gasparo Morticelli, M., & Sulli, A. (2020). Continental degassing of helium in an active tectonic setting (northern Italy): The role of seismicity. *Scientific Reports*, 10(1), 162. <https://doi.org/10.1038/s41598-019-55678-7>
- Caracausi, A., Buttitta, D., Picozzi, M., Paternoster, M., & Stabile, T. A. (2022). Earthquakes control the impulsive nature of crustal helium degassing to the atmosphere. *Communications Earth & Environment*, 3(1), 224. <https://doi.org/10.1038/s43247-022-00549-9>
- Caracausi, A., Favara, R., Italiano, F., Nuccio, P. M., Paonita, A., & Rizzo, A. (2005). Active geodynamics of the central Mediterranean Sea: Tensional tectonic evidence in western Sicily from mantle-derived helium. *Geophysical Research Letters*, 32(4), L04312. <https://doi.org/10.1029/2004GL021608>
- Caracausi, A., & Paternoster, M. (2015). Radiogenic helium degassing and rock fracturing: A case study of the southern Apennines active tectonic region. *Journal of Geophysical Research: Solid Earth*, 120(4), 2200–2211. <https://doi.org/10.1002/2014JB011462>
- Caracausi, A., & Sulli, A. (2019). Outgassing of mantle volatiles in compressional Tectonic regime away from volcanism: The role of Continental delamination. *Geochemistry, Geophysics, Geosystems*, 20(4), 2007–2020. <https://doi.org/10.1029/2018GC008046>
- Ciotoli, G., Bigi, S., Tartarello, C., Sacco, P., Lombardi, S., Ascione, A., & Mazzoli, S. (2013). Soil gas distribution in the main coseismic surface rupture zone of the 1980, Ms = 6.9, Irpinia earthquake (southern Italy). *Journal of Geophysical Research: Solid Earth*, 119(3), 2440–2461. <https://doi.org/10.1002/2013JB010508>
- Coltorti, M., Boraso, R., Mantovani, F., Morsilli, M., Fiorentini, G., Riva, A., et al. (2011). U and Th content in the Central Apennines continental crust: A contribution to the determination of the geo-neutrinos flux at LNGS. *Geochimica et Cosmochimica Acta*, 75(9), 2271–2294. <https://doi.org/10.1016/j.gca.2011.01.024>
- Coppola, L., & Pescatore, T. (1989). Lineamenti di neotettonica dei Monti Terminio-Tuoro, Cervialto e Marzano (Appennino meridionale). *Italian Journal of Geosciences*, 108, 105–119.
- Curzi, M., Aldega, L., Billi, A., Boschi, C., Carminati, E., Vignaroli, G., et al. (2024). Fossilchemical-physical (dis)equilibria between paleofluids and host rocks and their relationship to the seismic cycle and earthquakes. *Pre-proof Earth-Science Reviews*, 254, 104801. <https://doi.org/10.1016/j.earscirev.2024.104801>
- Curzi, M., Caracausi, A., Rossetti, F., Rabiee, A., Billi, A., Carminati, E., et al. (2022). From fossil to active hydrothermal outflow in the back-arc of the Central Apennines (Zannone Island, Italy). *Geochemistry, Geophysics, Geosystems*, 23(10). <https://doi.org/10.1029/2022GC010474>
- Dogan, T., Sumino, H., Nagao, K., Notsu, K., Tuncer, M. K., & Celik, C. (2009). Adjacent releases of mantle helium and soil CO<sub>2</sub> from active faults: Observations from the Marmara region of the North Anatolian Fault zone, Turkey. *Geochemistry, Geophysics, Geosystems*, 10(11). <https://doi.org/10.1029/2009GC002745>
- Dogliani, C., Harabaglia, P., Martinelli, G., Mongelli, F., & Zito, G. (1996). A Geodynamic model of the southern Apennines accretionary prism. *Terra Nova*, 8(6), 540–547. <https://doi.org/10.1111/j.1365-3121.1996.tb00783.x>
- Faulkner, D. R., & Armitage, P. J. (2013). The effect of tectonic environment on permeability development around faults and in the brittle crust. *Earth and Planetary Science Letters*, 375, 71–77. <https://doi.org/10.1016/j.epsl.2013.05.006>
- Ferraro, F., Agosta, F., Prasad, M., Vinciguerra, S., Violay, M., & Giorgioni, M. (2020). Pore space properties in carbonate fault rocks of peninsular Italy. *Journal of Structural Geology*, 130, 103913. <https://doi.org/10.1016/j.jsg.2019.103913>
- Gautheron, C., Moreira, M., & Allegre, C. (2005). He, Ne and Ar composition of the European lithospheric mantle. *Chemical Geology*, 217(1–2), 97–112. <https://doi.org/10.1016/j.chemgeo.2004.12.009>
- Gilfillan, S. M. V., Lollar, B. S., Holland, G., Blagburn, D., Stevens, S., Schoell, M., et al. (2009). Solubility trapping in formation water as dominant CO<sub>2</sub> sink in natural gas fields. *Nature*, 458(7238), 614–618. <https://doi.org/10.1038/nature07852>
- Giuffrida, A., Agosta, F., Rustichelli, A., Panza, E., La Bruna, V., Eriksson, M., et al. (2020). Fracture stratigraphy and DFN modelling of tight carbonates, the case study of the Lower Cretaceous carbonates exposed at the Monte Alpi (Basilicata, Italy). *Marine and Petroleum Geology*, 112, 104045. <https://doi.org/10.1016/j.marpetgeo.2019.104045>
- Goldstein, R. H. (2003). Petrographic analysis of fluid inclusions. In I. Samson, A. Anderson, & Marshall (Eds.), *Fluid inclusions: Analysis and interpretation: Mineralogical association of Canada* (Vol. D., pp. 1–45).
- Goodwin, N. R., Burgess, R., Craw, D., Teagle, D. A., & Ballentine, C. J. (2017). Noble gases fingerprint a metasedimentary fluid source in the Macraes orogenic gold deposit, New Zealand. *Mineralium Deposita*, 52(2), 197–209. <https://doi.org/10.1007/s00126-016-0648-x>
- Gori, F., Paternoster, M., Barbieri, M., Buttitta, D., Caracausi, A., Parente, F., et al. (2023). Hydrogeochemical multi-component approach to assess fluids upwelling and mixing in shallow carbonate-evaporitic aquifers (Contursi area, southern Apennines, Italy). *Journal of Hydrology*, 618, 129258. <https://doi.org/10.1016/j.jhydrol.2023.129258>
- Graham, D. W. (2002). Noble gas isotope geochemistry of mid-ocean ridge and Ocean Island Basalts: Characterization of mantle source reservoirs. *Reviews in Mineralogy and Geochemistry*, 47(1), 247–317. <https://doi.org/10.2138/rmg.2002.47.8>
- Gratier, J. P., & Gamond, J. F. (1990). Transition between seismic and aseismic deformation in the upper crust. *Geological Society of London*, 54(1), 461–473. <https://doi.org/10.1144/GSL.SP.1990.054.01.42>
- Hancock, P. L., & Barka, A. A. (1987). Kinematic indicators on active normal faults in western Turkey. *Journal of Structural Geology*, 9(5/6), 573–584. [https://doi.org/10.1016/0191-8141\(87\)90142-8](https://doi.org/10.1016/0191-8141(87)90142-8)
- Honda, M., Kurita, K., Hamano, Y., & Ozima, M. (1982). Experimental studies of He and Ar degassing during rock fracturing. *Earth and Planetary Science Letters*, 59(2), 429–436. [https://doi.org/10.1016/0012-821X\(82\)90144-3](https://doi.org/10.1016/0012-821X(82)90144-3)



- Italiano, F., Martelli, M., Martinelli, G., & Nuccio, P. M. (2000). Geochemical evidence of melt intrusions along lithospheric faults of the Southern Apennines, Italy: Geodynamic and seismogenic implications. *Journal of Geophysical Research*, *105*(B6), 3569–3578. <https://doi.org/10.1029/2000JB900047>
- Kendrick, M. A., & Burnard, P. (2013). Noble gases and halogens in fluid inclusions: A journey through the Earth's crust. In *The noble gases as geochemical tracers* (pp. 319–369). Springer. [https://doi.org/10.1007/978-3-642-28836-4\\_11](https://doi.org/10.1007/978-3-642-28836-4_11)
- Kulongoski, J. T., Hilton, R. D., Barry, P. H., Esser, B. K., Hillegonds, D., & Belitz, K. (2013). Volatile fluxes through the big bend section of the San Andreas Fault, California: Helium and carbon-dioxide systematics. *Chemical Geology*, *339*, 92–102. <https://doi.org/10.1016/j.chemgeo.2012.09.007>
- Lee, J. Y., Marty, K., Severinghaus, J. P., Kawamura, K., Yoo, H.-S., Lee, J. B., & Kim, J. S. (2006). A redetermination of the isotopic abundances of atmospheric Ar. *Geochimica et Cosmochimica Acta*, *70*(17), 4507–4512. <https://doi.org/10.1016/j.gca.2006.06.1563>
- Liu, W., Zhang, M., Chen, B., Liu, Y., Cao, C., Xu, W., et al. (2023). Hydrothermal He and CO<sub>2</sub> degassing from a Y-shaped active fault system in eastern Tibetan Plateau with implications for seismogenic processes. *Journal of Hydrology*, *620*(B), 129482. <https://doi.org/10.1016/j.jhydrol.2023.129482>
- Mabry, J., Lan, T., Burnard, P., & Bernard, M. (2013). High-precision helium isotope measurements in air. *Journal of Analytical Atomic Spectrometry*, *28*(12), 1903–1910. <https://doi.org/10.1039/c3ja50155h>
- Manniello, C., Abdallah, I. B., Prosser, G., & Agosta, F. (2023). Pressure solution-assisted diagenesis and thrusting-related deformation of Mesozoic platform carbonates. *Journal of Structural Geology*, *173*, 104906. <https://doi.org/10.1016/j.jsg.2023.104906>
- Marchesini, B., Carminati, E., Aldega, L., Mirabella, F., Petrelli, M., Caracausi, A., & Barchi, M. R. (2022). Chemical interaction driven by deep fluids in the damage zone of a seismogenic carbonate fault. *Journal of Structural Geology*, *161*, 104668. <https://doi.org/10.1016/j.jsg.2022.104668>
- O'Nions, R. K., & Oxburgh, E. R. (1988). Helium volatile fluxes and the development of continental crust. *Earth and Planetary Science Letters*, *90*(3), 331–347. [https://doi.org/10.1016/0012-821X\(88\)90134-3](https://doi.org/10.1016/0012-821X(88)90134-3)
- O'Nions, R. K., & Oxburn, E. H. (1983). Heat and helium in the Earth. *Nature*, *306*(5942), 429–431. <https://doi.org/10.1038/306429a0>
- Ozima, M., & Podosek, F. A. (2002). *Noble gas geochemistry*. Cambridge University Press. <https://doi.org/10.1017/cbo9780511545986>
- Passchier, C. W., & Trouw, R. A. J. (2005). *Microtectonic*. Springer Berlin Heidelberg.
- Patacca, E., Sartori, R., & Scandone, P. (1990). Tyrrhenian Basin and Apenninic arcs: Kinematic relations since late Tortonian times. *Italian Journal of Geosciences*, *45*, 425–451.
- Patacca, E., & Scandone, P. (2007). Geology of the Southern Apennines. *Bollettini Società Geologica Italiana*, *7*, 75–119.
- Pik, R., & Marty, B. (2009). Helium isotopic signature of modern and fossil fluids associated with the Corinth rift fault zone (Greece): Implication for fault connectivity in the lower crust. *Chemical Geology*, *266*(1–2), 67–75. <https://doi.org/10.1016/j.chemgeo.2008.09.024>
- Randazzo, P., Caracausi, A., Aiuppa, A., Cardellini, C., Chiodini, G., D'Alessandro, W., et al. (2021). Active degassing of deeply sourced fluids in central Europe: New evidences from a geochemical study in Serbia. *Geochemistry, Geophysics, Geosystems*, *22*(11), e2021GC010017. <https://doi.org/10.1029/2021GC010017>
- Rizzo, A. L., Faccini, B., Casetta, F., Faccincani, L., Ntaflou, T., Italiano, F., & Coltorti, M. (2021). Melting and metasomatism in West Eifel and Siebengebirge Sub Continental Lithospheric Mantle: Evidence from concentrations of volatiles in fluid inclusions and petrology of ultramafic xenoliths. *Chemical Geology*, *581*, 120400. <https://doi.org/10.1016/j.chemgeo.2021.120400>
- Rizzo, A. L., Pelorosso, B., Coltorti, M., Ntaflou, T., Bonadiman, C., Malek, M. M., et al. (2018). Geochemistry of Noble Gases and CO<sub>2</sub> in fluid inclusion from lithospheric mantle Beneath Wilcza Gora (Lower Silesia, Southwest Poland). *Frontiers in Earth Sciences*, *6*, 215. <https://doi.org/10.3389/feart.2018.00215>
- Rizzo, A. L., Uysal, I. T., Mutlu, H., Unal-Imer, E., Dirik, K., Yuce, G., et al. (2019). Geochemistry of fluid inclusions in travertines from Western and Northern Turkey: Inferences on the Role of Active faults in fluids circulation. *Geochemistry, Geophysics, Geosystems*, *20*(11), 5473–5498. <https://doi.org/10.1029/2019GC008453>
- Sano, Y., & Marty, B. (1995). Origin of carbon in fumarolic gas from island arcs. *Chemical Geology*, *119*(1–4), 265–274. [https://doi.org/10.1016/0009-2541\(94\)00097-R](https://doi.org/10.1016/0009-2541(94)00097-R)
- Sano, Y., Takahata, N., Igarashi, G., Koizumi, N., & Sturchio, N. C. (1998). Helium degassing related to the Kobe earthquake. *Chemical Geology*, *150*(1–2), 171–179. [https://doi.org/10.1016/S0009-2541\(98\)00055-2](https://doi.org/10.1016/S0009-2541(98)00055-2)
- Sano, Y., Takahata, N., Kagoshima, T., Shibada, T., Onoue, T., & Zhao, D. (2016). Groundwater helium anomaly reflects strain change during the 2016 Kumamoto earthquake in Southwest Japan. *Scientific Reports*, *6*(1), 37939. <https://doi.org/10.1038/srep37939>
- Sano, Y., Wakita, H., Ohsumi, T., & Kusakabe, M. (1987). Helium isotope evidence for magmatic gases in Lake Nyos, Cameroon. *Geophysical Research Letters*, *14*(10), 1039–1041. <https://doi.org/10.1029/GL014i010p01039>
- Shiner, P., Beccacini, A., & Mazzoli, S. (2004). Thin-skinned versus thick-skinned structural models for Apulian carbonate reservoir: Constraint from the Val d'Agri Fields, S. Apennines, Italy. *Marine and Petroleum Geology*, *21*, 805–827. <https://doi.org/10.1016/j.marpetgeo.2003.11.020>
- Sibson, R. H. (2000). Fluid involvement in normal faulting. *Journal of Geodynamics*, *29*(3–5), 469–499. [https://doi.org/10.1016/S0264-3707\(99\)00042-3](https://doi.org/10.1016/S0264-3707(99)00042-3)
- Slejko, D., Peruzza, L., & Rebez, A. (1998). Seismic hazard maps of Italy. *Annals of Geophysics*, *41*(2). <https://doi.org/10.4401/ag-4327>
- Smeraglia, L., Bernasconi, S. M., Berra, F., Billi, A., Boschi, C., Caracausi, A., et al. (2018). Crustal-scale fluid circulation and co-seismic shallow comb-veining along the longest normal fault of the central Apennines, Italy. *Earth and Planetary Science Letters*, *498*, 152–168. <https://doi.org/10.1016/j.epsl.2018.06.013>
- Smeraglia, L., Berra, F., Billi, A., Boschi, C., Carminati, E., & Doglioni, C. (2016). Origin and role of fluids involved in the seismic cycle of extensional faults in carbonate rocks. *Earth and Planetary Science Letters*, *450*, 292–305. <https://doi.org/10.1016/j.epsl.2016.06.042>
- Smeraglia, L., Fabbri, O., Choulet, F., Jaggi, M., & Bernasconi, S. M. (2022). The role of thrust and strike-slip faults in controlling regional-scale paleofluids circulation in fold-and-thrust belt: Insights from the Jura Mountains (eastern France). *Tectonophysics*, *829*, 229299. <https://doi.org/10.1016/j.tecto.2022.229299>
- Stewart, I. S., & Hancock, P. L. (1990). Brecciation and fracturing within neotectonic normal fault zones in the Aegean region. *Geological Society, London*, *54*(1), 105–110. <https://doi.org/10.1144/GSL.SP.1990.054.01.11>
- Tang, Y., Bi, X., Fayek, M., Stuart, F. M., Wu, L., Jiang, G., et al. (2017). Genesis of the Jinding Zn-Pb deposit, northwest Yunnan Province, China: Constraints from rare Earth elements and noble gas isotopes. *Ore Geology Reviews*, *90*, 970–986. <https://doi.org/10.1016/j.oregeorev.2017.04.024>
- Tantillo, M., Riccobono, G., & Rizzo, A. L. (2009). *Sistema di frantumazione minerali e rocce (crusher) per la stima delle concentrazioni elementari ed isotopiche dei gas nobili contenuti nelle inclusioni fluide*. Rapporti tecnici INGv.

- Todaro, S., Manniello, C., Pietragalla, A., Preto, N., & Agosta, F. (2024). Depositional Setting diagenetic processes, and pressure solution-assisted compaction of Mesozoic Platform carbonate, southern Apennines, Italy. *Geosciences*, *14*(4), 89. <https://doi.org/10.3390/geosciences14040089>
- Torgensen, T. (2010). Continental degassing flux of  $^4\text{He}$  and its variability. *Geochemistry, Geophysics, Geosystems*, *11*, 6. <https://doi.org/10.1029/2009GC002930>
- Vezzani, L., Festa, A., & Ghisetti, F. (2010). Geological-structural map of the central-southern Apennine (Italy). *Geological Society of America*, *469*. <https://doi.org/10.1130/2010.2469>
- Wu, L. Y., Hu, R. Z., Li, X. F., Stuart, F. M., Jiang, G. H., Qi, Y. Q., & Zhu, J. J. (2018). Mantle volatiles and heat contributions in high sulfidation epithermal deposit from the Zijinshan Cu-Au-Mo-Ag orefield, Fujian Province, China: Evidence from He and Ar isotopes. *Chemical Geology*, *480*, 58–65. <https://doi.org/10.1016/j.chemgeo.2017.08.005>
- Zhang, M., Guo, Z., Xu, S., Barry, P. H., Sano, Y., Zhang, L., et al. (2021). Linking deeply-sourced volatile emissions to plateau growth dynamics in southeastern Tibetan Plateau. *Nature Communications*, *12*(1), 4157. <https://doi.org/10.1038/s41467-021-24415-y>